MLIB: an easy-to-use Matlab toolbox for the analysis of extracellular spike data

Maik C. Stüttgen

Affiliation: Institute of Pathophysiology, University Medical Center of the Johannes Gutenberg University Mainz, Mainz, Germany

Keywords: neurophysiology, electrophysiology, action potential, local field potential, in vivo, peri-stimulus time histogram, spike density function, area under the ROC curve

Correspondence:

Maik C. Stüttgen

University Medical Center Mainz

Institute of Pathophysiology

Duesbergweg 6

51128 Mainz

Germany

Email: maik.stuettgen@uni-mainz.de

Phone: +49 6131 39 21905

Abstract

The analysis of neurophysiological data obtained from extracellular recordings is usually performed using a number of standard techniques. These include a) the extraction of action potentials from voltage traces and their subsequent classification, i.e., spike sorting, b) the visualization of activity, e.g., by constructing raster plots, peri-stimulus time histograms (PSTHs), and spike density functions, and c) the quantification of neuronal responses according to experimental variables such as stimulation or movement. Here I present a Matlab toolbox containing functions for the visualization and analysis of neuronal spike data. The toolbox consists entirely of one-liners that operate on vector or matrix inputs, i.e., spike and event timestamps or waveform samples. The toolbox functions provide both basic (constructing PSTHs, computing waveform characteristics etc.) and more advanced functionality, such as dimensionality reduction of multi-neuron recordings. While offering a high degree of versatility, the toolbox should also be accessible to newcomers to neurophysiology, such as (under)graduate students or PhD students. The functions are easy to use, and each function is extensively introduced with several examples using real or simulated data. In addition, many functions provide fully formatted plots on request, even with minimal Matlab knowledge. The toolbox is available from https://github.com/maikstue/mlib-spike-data.

Introduction

The extracellular observation of neurons' electrical activity constitutes one of the most powerful methods to investigate brain function. One hundred years after the first recordings of extracellular action potentials in mammals (Adrian, 1926), researchers can now record up to several thousand neurons simultaneously (Kleinfeld et al., 2019; Steinmetz et al., 2021), providing an unprecedented opportunity to investigate the workings of the brain in real time. Insights gained from this technique include the principles of neural information processing such as rate and temporal coding, feature selectivity, adaptation, and gain modulation (Adrian, 1926; DeCharms and Merzenich, 1996; Lettvin et al., 1959; Salinas and Thier, 2000). In consequence, today extracellular spike recordings are a cornerstone of neuroscience research, and are applied to a wide variety of research questions, including sensory processing, attention and cognition, decision-making, sensorimotor control, learning and memory, as well as applied research directed towards the development of brain-computer interfaces and neuroprosthetics.

The analysis of neurophysiological data obtained through extracellular recordings is typically conducted using a range of standard techniques. These include a) spike extraction and sorting, i.e., the close inspection of spike waveforms to identify and eliminate artifacts, and the waveforms' subsequent clustering to obtain single-unit spike trains from multi-unit recordings; b) the visualization of neural activity, for example through the construction of raster plots, peri-stimulus time histograms (PSTHs), and spike density functions (SDFs); and c) the quantification of neural responses according to experimental variables such as stimulation or movement to test research hypotheses. Such analyses are usually performed with custom-written code, predominantly written in Matlab or Python, although many labs also rely on either commercially available software packages or freely available toolboxes (reviewed in (Unakafova and Gail, 2019)).

In many labs, neuronal spike data is obtained frequently by master or PhD students with little or no programming experience and limited knowledge of typical analysis procedures for neuronal spike data. (In my experience, even many experienced postdoctoral research fellows struggle with

the analysis of spike data.) To provide such users with an accessible, easy-to-use solution for most standard analysis scenarios, I created a Matlab toolbox specifically for that purpose. The toolbox contains 17 functions to visualize and analyze neuronal spike data, and three additional functions pertaining to local field potential data. The toolbox functions not only cover the most basic spike analyses, such as constructing raster plots, PSTHs, and SDFs, but also more advanced and specialized analyses, among them time-resolved multiple regression of firing rates on experimental variables, clustering of multiple neurons' PSTHs to categorize neurons into subclasses, and dimensionality reduction of multi-neuron recordings to visualize population activity. By design, the functions are easy to use for newcomers: all functions can be called directly from Matlab's Command Window, and the use of each function is illustrated with several examples, drawing on real data recorded in rats, mice, and pigeons.

Overview

The MLIB functions have been developed over the past decade and tested using Matlab R2023b on a standard desktop PC running Windows 11. The example data are in part taken from previous studies and include spike recordings performed in rats, mice, and pigeons (Kasties et al., 2016; Lengersdorf et al., 2014; Starosta et al., 2014, 2013; Stoilova et al., 2020; van der Bourg et al., 2017; Vandevelde et al., 2023; Yeganeh et al., 2022). Table 1 lists all MLIB functions in alphabetical order and provides brief descriptions. Beyond the basic Matlab installation, some functions require the Statistics and Machine Learning Toolbox; one function (**mtune.m**) requires the Curve Fitting and Signal Processing Toolboxes.

MLIB is designed to allow conducting basic electrophysiological analyses with a minimum of MATLAB knowledge. The library does not require installation, the user simply needs to copy the functions and example data files into a folder and then add that folder to the MATLAB user path. All functions are one-liners and operate directly on vector or array input. Customization of the functions' outputs is achieved through the provision of input arguments, which are explained in each function's introductory comments (type 'doc' and then the name of the function to read it). Additionally, a function reference script with several usage demonstrations for each function is provided to facilitate quick understanding of how the functions work. All results figures in this manuscript can be reproduced using the reference script.

For a broad introduction into the analysis of neuronal signals in general, the reader is referred to a freely available Matlab tutorial (Chakrabarti, 2024).

Table 1: Overview over MLIB functions in alphabetical order.

Function name	Primary input data	Brief description
mcc[1]	spike waveforms from two or more clusters; spike time stamps	visualizes unit clusters and provides quality metrics to quantify spike sorting success
mcheck[1]	spike waveforms from one unit cluster; spike time stamps	visualizes one unit's waveforms and provides quality metrics
mcluster[1]	PSTHs from different units	clusters PSTHs from different units according to their similarity
mcsd	LFP data from a linear electrode array, averaged over multiple identical trials	performs a current source density analysis and plots the result
mcvar	spike time stamps from a single unit	computes the coefficient of variation for interspike intervals and the Fano factor for spike counts
mdimreduct[1]	PSTHs from different units	performs dimensionality reduction of spike responses from several units recorded under the same conditions
mep[1]	continuous local LFP data from a single or multiple electrodes	returns the evoked potential with error bars and confidence intervals
mlat[1]	spike and event time stamps	provides several measures of response latency
mmi[1]	spike counts obtained from the same unit under two different conditions	computes mutual information of spike counts
mmi_psych[1]	behavioral performance indices (hit rate and false alarm rate)	expresses behavioral performance in bits to compare with neuronal MI
mmultregress[1]	spike and event time stamps	performs a sliding-window multiple regression analysis of spike responses
mnspx	spike and event time stamps	provides a vector of spike counts in an interval around a series of events
mpsth	spike and event time stamps	constructs a PSTH and raster plot
mroc[1]	spike counts obtained from the same unit under two different conditions	computes the area under the ROC curve (AUROC) for two spike count distributions
msdf[1]	PSTH from one unit	constructs a spike-density function from a PSTH
mspectan	continuous LFP data	performs spectral analysis of LFP data
mtune[2,3]	spike and event time stamps	constructs and fits a tuning curve
mvecstrength	spike and event time stamps	computes vector strength of a spike response relative to a periodic signal
mwa[1]	spike and event time stamps	computes a 'window analysis', i.e., AUROC of a spike train in moving windows relative to a fixed reference event
mwa2[1]	spike and event time stamps	computes a 'window analysis', i.e., AUROC of two spike trains e.g., relative to two different stimuli
mwave	spike waveforms from a single unit	plots the average spike waveform and computes its characteristics (peak-to-trough duration etc.)

[1] requires the Statistics and Machine Learning Toolbox

[2] requires the Curve Fitting Toolbox

[3] requires the Signal Processing Toolbox

Illustration

The analysis of extracellular spike recordings typically involves a series of analysis steps which are outlined in Figure 1. I will introduce several MLIB functions with reference to the analysis flow shown in this figure. Note that each function has features not illustrated in this paper; the full scope is described in detail in each function's documentation and illustrated with example data in an accompanying function reference script. All experiments performed on animals were conducted in accordance with the German guidelines for the care and use of animals in science as well as with the Directive 2010/63/EU of the European Parliament and of the Council of 22 September 2010 concerning the care and use of animals for experimental purposes, and all procedures were approved by national ethics committees of the states of North Rhine-Westphalia (LANUV) and Rhineland-Palatinate (LUA), Germany (Az. 8.87-50.10.37.09.277, G 19-1-094, G 19-1-085).

Checking the quality of spike sorting

The MLIB toolbox does not contain functions for spike sorting per se, as there are already multiple excellent free spike sorting packages available (Hill et al., 2011; Pachitariu et al., 2024; Quian Quiroga et al., 2009; Rossant et al., 2016), in addition to some commercial software packages (e.g., Plexon's Offline Sorter and CED's Spike2). That said, MLIB provides functions which aid in assessing the quality of sorting post-hoc by providing several useful analyses.

These functions are illustrated in Figure 2 which shows several panels taken from the MLIB functions **mcheck**, **mcc**, and **mwave**. Sample waveforms of an example single unit recorded in the pigeon nidopallium caudolaterale (NCL; (Starosta et al., 2014)) are shown in Figure 2A, along with the mean and ±2 standard deviations. Figure 2B shows the same data, but expressed as a heat map of time-voltage values. Such heat maps can aid in the identification of multi-units (i.e., spikes from two or more neurons inadvertently lumped together in the same unit; see reference script for an example). Another indication for a multi-unit is a bimodal distribution of waveform peaks such as those shown in Figure 2C. The blue distribution represents the noise distribution for reference, the

green (red) distribution represents all waveforms' minimum (maximum) values. As this unit's spike amplitude detection threshold was negative (vertical dotted line), primarily the green distribution is of relevance (for spikes with positive peaks, the red distribution would be more relevant). A Gaussian curve (black) is fitted to the amplitude distribution and serves to estimate the frequency of false negative spikes. Assuming normally distributed waveform amplitudes, there is a conspicuous lack of spikes in the rightmost tail of the distribution (arrow). For this example, it is estimated that 2% of spikes escaped detection. Figure 2D shows the inter-spike interval (ISI) distribution for this unit. ISIs of less than 3-4 ms indicate violation of the action potential refractory period and are not consistent with all spikes originating from the same neuron. For this unit, less than 0.5 % of spikes violate this criterion, which is a commonly used value to denote a unit as "single unit" (e.g., (Reyes-Puerta et al., 2015).

Figures 2E through 2G are useful to assess the stability of the recording. While action potential recordings with chronically implanted microwires are usually stable over several hours, acute recordings with single electrodes or electrode arrays tend to be less stable because of electrode drift or movements of the animal e.g. in head-fixed settings. Figure 2E shows cumulated spikes as a function of time; a perfectly stable unit would be expected to have a curve very close to the main diagonal of the figure (black dotted line). However, neuronal firing rates in many brain areas are expected to vary as a function of experimental parameters, e.g. when recording from behaving animals. In that case, cumulated spikes are less informative about recording stability, but the change in waveform amplitude is (shown in Figure 2F as a function of time). Figure 2G allows combined assessment of firing rate (black histogram with 1-min bins) and spike amplitude (red dots). **mcheck** also provides two quantitative measures to gauge unit stability (CV(amps) and CV(fr), which are explained in the function reference). Assessing unit stability is of paramount importance especially when neurons are observed under various conditions which change blockwise, as for example in some behavioral studies (Elber-Dorozko and Loewenstein, 2018). The function also provides some metrics useful for quantitative evaluation and selection of units for further analyses, along with three-stage recommendations (symbolized with traffic lights and easily customizable;

Figure 2H). Finally, Figure 2I shows how the function **mwave** extracts basic waveform properties to assist in the classification into e.g. putative excitatory and inhibitory neurons (full width at half maximum, peak-to-trough duration etc.; (McCormick et al., 1985)).

While **mcheck** focuses on signal quality of a single waveform cluster, the function **mcc** allows to assess the separability of two or more spike clusters. In the present example, waveforms from a single electrode were clustered into two groups. Figure 2J shows spikes from the two clusters superimposed and color-coded for visual inspection. Waveforms from both clusters were subjected to principal component analysis, and Figure 2K shows the first three principal principal components for all waveforms. **mcc** offers several quantitative cluster separability indices. Figure 2L provides an intuitive depiction of the classification performance (along with the non-parametric area under the curve A' which should approximate 1; a value of 0.5 signifies complete overlap of the two clusters). The x-axis represents the difference of the distances of each spike from its cluster center and to the center of the other cluster. If all spikes are closer to their respective cluster center than to that of the other cluster, the two distributions are completely separated and do not include 0, and A'=1 (note the logarithmic scaling of the ordinate). Other widely used quantitative indices provided by **mcc** include J3, PseudoF, DBVI, L_{ratio}, and isolation distance (Nicolelis et al., 2003; Schmitzer-Torbert et al., 2005), see Figure 2M.

Single-neuron spike train analysis

After spike sorting is finished, the next analysis step is typically to visualize the response characteristics of a unit by means of a peri-stimulus time histogram (PSTH) and an event-triggered raster display (Figure 3A, constructed with **mpsth**). As PSTHs are inherently noisy due to limited recording durations, the instantaneous firing rate is frequently estimated through convolution of the PSTH with a filtering kernel, yielding the so-called spike density function (SDF). Figure 3A shows an SDF obtained from convolution of the PSTH with an exponentially modified Gaussian kernel (yellow line) obtained through **msdf** (the function also offers boxcar, Gaussian, and simple exponential kernels of arbitrary width). Figure 3A also illustrates the output of the function **mlat** which can be

used to estimate a unit's response latency relative to a certain event (colored dots plotted over the peak of the SDF). **mlat** offers five common measures of response latency, and three of these are shown in Figure 3A.

Especially in sensory neurophysiology, precise estimation of the timing and content of information in a spike train is of interest. This can be achieved through the functions **mwa** and **mwa2**. Figure 3B shows the output of **mwa**, computed for the same neuron as depicted in Figure 3A. Analysis windows of varying duration (ranging from 5 to 100 ms) were shifted in steps of 10 ms relative to the onset of the stimulus at time point 0. In each analysis window, the area under the receiver operating characteristic (ROC) curve (AUROC) is computed for spike counts in the analysis windows against spike counts in a reference window (here, pre-stimulus baseline) of the same duration. The heat map in Figure 3B shows that the maximum change in firing rate is present within 20-30 ms after stimulus onset. From a readout perspective, the optimal (AUROC-maximizing) analysis window duration is 50 ms, centered at +20 ms (AUROC=0.77; the window is highlighted by an asterisk in the figure). Such information is useful to understand how downstream brain areas might read out information from sensory representations for decision-making (Stüttgen and Schwarz, 2010, 2008). An alternative measure for AUROC is mutual information, which can be computed via the function **mmi** (Panzeri and Treves, 1996; Treves and Panzeri, 1995).

A frequently employed technique to examine the coding properties of single neurons is multiple regression. The general idea is that a neuron's spike counts can be influenced by several factors which can be difficult to disentangle experimentally (e.g., (Kim et al., 2009; Romo et al., 2002). For example, we recorded single neurons from rat dorsomedial frontal cortex (dMFC) while the animal was performing a two-stimulus auditory forced-choice discrimination task (Stoilova et al., 2020). In each of 160 trials, one out of two 100-ms auditory stimuli (noise bursts) differing in frequency content was presented when the animal's snout entered a centrally located nose port. The animal had to wait until 50 ms after stimulus offset and then was free to withdraw and move into either of two laterally located choice ports. Following stimulus (S) 1, the animal received reward when entering the right choice port, following S2, reward was obtained when the animal entered the

left choice port. The rats classified the stimuli correctly in around 80% of trials. We asked whether dMFC firing rates reflected stimulus identity, the choice response, or their interaction (reward or time-out punishment). Moreover, we asked at what time point(s) during the trial epochs dMFC neurons represent this information. We used the function **mmultregress** to perform this analysis, regressing single-neuron spike counts (the criterion variable) in 25-, 100-, and 250-ms windows shifted smoothly relative to stimulus onset (Figure 3C). Predictor variables were stimulus identity (S1 or S2), the choice response (right or left), and reward (yes or no; signed-effects coding, i.e., -1 vs. +1). The results are shown in Figure 3C. The top panels show the weights for the three regressors as a function of analysis window position, the bottom panels show the squared semipartial correlation coefficients (r_{sp}^2) of each predictor. It is evident that this neuron mainly represents the animal's choice response (red curves), starting around 250 ms after stimulus onset. Regression weights and r_{sp}^2 values are generally larger and less noisy with longer analysis windows (at the expense of temporal resolution). Generally speaking, r_{sp}^2 represents the unique fraction of variance explained by any regressor, purified from its correlation with the other regressors, which can aid the interpretation of the effect of the independent variables (Cohen et al., 2003).

Population analysis through dimensionality reduction

In recent years, due to technological advancements which allow to simultaneously record from large numbers of neurons (Steinmetz et al., 2021), the focus of neurophysiologists has shifted from the classic analysis of single-neuron spike trains and across-neuron averages to the visualization of population activity trajectories in multiple dimensions (Ebitz and Hayden, 2021; Saxena and Cunningham, 2019). The function **mdimreduct** accepts averaged spike counts from N neurons, performs PCA-based dimensionality reduction, and plots the resultant population activity trajectory in 2- and 3-dimensional space. Figure 4A visualizes the input array to the function – z-scored firing rates in 100-ms analysis windows for 300 dMFC neurons, aligned to the onset of stimulus 1 (same auditory discrimination task as described in the previous section). Neural activity was taken from 400 ms before until 400 ms after stimulus onset (correct trials only). This matrix was subjected to

principal component analysis. Figure 4B shows the scores of the first 16 principal components (PCs), Figure 4C shows explained variance cumulated over the first 16 PCs. As frequently observed with this kind of data, the 300-dimensional activity vector which served as the input can be safely reduced to a handful of PCs (the first 5 PCs explain almost 80% of the total variance). Figure 4D shows the population trajectory for the first three PCs for correct S1 trials. Time relative to stimulus onset is color-coded, with darker points representing earlier and lighter dots representing later time points. When the data matrix from Figure 4A for S1 is concatenated with the corresponding matrix for S2 (not shown) and the concatenated matrix is then subjected to PCA, population trajectories for the two types of trials – S1 presentations followed by movement to the right, S2 presentations followed by movement to the left – can be visualized together as in Figure 4E. Before stimulus onset, the two trajectories are virtually identical. Shortly after stimulus onset, the two trajectories diverge (arrow) as the animal makes its decision to move to either of the two choice ports. This divergence is observed already before the stimulus has ended and the animal has withdrawn from the center port, indicating early involvement of the dMFC population in the decision process and/or response planning.

Analysis of local field potentials

While the vast majority of MLIB functions are concerned for spike train analysis, three functions are useful for analyzing local field potential (LFP) data (**mcsd**, **mep**, **mspectan**). Here, I will introduce only the function **mcsd** which computes and plots the results of a current-source density (CSD) analysis. CSD is a useful tool to assign individual contacts from linear electrode arrays to cortical layers (Vandevelde et al., 2023; Yang et al., 2017; Yeganeh et al., 2022). Figure 5A depicts averaged LFP (voltage) traces from 20 linearly spaced electrodes (inter-electrode distance 50 µm) inserted into the barrel cortex of an anesthetized mouse (van der Bourg et al., 2017). The position of the electrode is color-coded (black: topmost electrode contact, white: lowermost electrode contact). A single sinusoidal whisker stimulus was applied, starting at time point 0. LFPs were averaged over 20 trials. Figure 4B shows the same data as in 4A as a heat map, highlighting that the strongest LFP response was observed at the 5th contact from the top. Figure 4C shows the raw CSD (i.e., the second

spatial derivative of the LFP in Figure 4B). The raw CSD was then spatially interpolated 10-fold and smoothed (Figure 4D) to allow easier identification of the earliest current sink (white arrow) which can be used to identify layer IV, allowing precise assignment of electrode contacts (and the units recorded with them). The other electrode contacts can then be assigned to the remaining layers through the combined consideration of the current sources and histological references (Mitzdorf, 1985; Reyes-Puerta et al., 2015).

Conclusion

In summary, MLIB is an easy-to-use yet versatile open-source toolbox for the analysis of extracellular spike and field potential data. Through detailed documentation and usage demonstrations in an accompanying Matlab Live Script, it should be useful for both beginners and more experienced experimentalists in need of basic as well as some more advanced analysis functions. For more specialized analysis techniques, especially for large-scale neuronal recordings, the reader is referred to (Stringer et al., 2025; Stringer and Pachitariu, 2024). For comprehensive overviews of spike and LFP analysis toolboxes written in Matlab and Python, see (Unakafova and Gail, 2019) and the SpikeResources collection on GibtHub (https://github.com/openlists/SpikeResources).

With the advent of large-scale multi-neuron recording techniques, analysis techniques will continue to evolve (Stringer and Pachitariu, 2024). However, the basic visualization and analysis of the single-neuron response properties is likely to remain an important starting point for the analysis of electrophysiological data. I hope that experimentalists will continue to appreciate the easy-to-use functions provided by MLIB to get started exploring their spike data.

References

Adrian, E.D., 1926. The impulses produced by sensory nerve endings: Part I. J Physiol 61, 49–72. https://doi.org/10.1113/jphysiol.1926.sp002273

Chakrabarti, S., 2024. Electrophysiology Tutorial for Neuroscience [WWW Document]. URL https://github.com/MathWorks-Teaching-Resources/Electrophysiology-Tutorial-for-Neuroscience/releases/tag/v1.2 (accessed 11.20.24).

Cohen, J., Cohen, P., West, S.G., Aiken, L.S., 2003. Applied multiple regression/correlation analysis for the behavioral sciences, 3rd ed. Taylor & Francis Group.

DeCharms, R.C., Merzenich, M.M., 1996. Primary cortical representation of sounds by the coordination of action-potential timing. Nature 381, 610–613.

Ebitz, R.B., Hayden, B.Y., 2021. The population doctrine in cognitive neuroscience. Neuron 109, 3055–3068. https://doi.org/10.1016/j.neuron.2021.07.011

Elber-Dorozko, L., Loewenstein, Y., 2018. Striatal Action-Value Neurons Reconsidered. Elife 7, e34248. https://doi.org/10.1101/087502

Hill, D.N., Mehta, S.B., Kleinfeld, D., 2011. Quality metrics to accompany spike sorting of extracellular signals. Journal of Neuroscience 31, 8699–705. https://doi.org/10.1523/JNEUROSCI.0971-11.2011

Kasties, N., Starosta, S., Güntürkün, O., Stüttgen, M.C., 2016. Neurons in the pigeon caudolateral nidopallium differentiate Pavlovian conditioned stimuli but not their associated reward value in a sign-tracking paradigm. Sci Rep 6, 35469. https://doi.org/10.1038/srep35469

Kim, H., Sul, J.H., Huh, N., Lee, D., Jung, M.W., 2009. Role of striatum in updating values of chosen actions. Journal of Neuroscience 29, 14701–14712. https://doi.org/10.1523/JNEUROSCI.2728-09.2009

Kleinfeld, D., Luan, L., Mitra, P.P., Robinson, J.T., Sarpeshkar, R., Shepard, K., Xie, C., Harris, T.D., 2019. Can One Concurrently Record Electrical Spikes from Every Neuron in a Mammalian Brain? Neuron 103, 1005–1015. https://doi.org/10.1016/j.neuron.2019.08.011

Lengersdorf, D., Pusch, R., Güntürkün, O., Stüttgen, M.C., 2014. Neurons in the pigeon nidopallium caudolaterale signal the selection and execution of perceptual decisions. European Journal of Neuroscience 40, 3316–27.

Lettvin, J.Y., Maturana, H.R., McCulloch, W.S., Pitts, W.H., 1959. What the frog's eye tells the frog's brain. Proceedings of the IRE 47, 1940–1951.

McCormick, D.A., Connors, B.W., Lighthall, J.W., Prince, D.A., 1985. Comparative Electrophysiology of Pyramidal and Sparsely Spiny Stellate Neurons of the Neocortex. J Neurophysiol 54, 782–806.

Mitzdorf, U., 1985. Current source-density method and application in cat cerebral cortex: investigation of evoked potentials and EEG phenomena. Physiol Rev 65, 37–100. https://doi.org/n/a

Nicolelis, M.A.L., Dimitrov, D., Carmena, J.M., Crist, R., Lehew, G., Kralik, J.D., Wise, S.P., 2003. Chronic, multisite, multielectrode recordings in macaque monkeys. Proc Natl Acad Sci U S A 100, 11041–11046. https://doi.org/10.1073/pnas.1934665100

Pachitariu, M., Sridhar, S., Pennington, J., Stringer, C., 2024. Spike sorting with Kilosort4. Nat Methods 21, 914–921. https://doi.org/10.1038/s41592-024-02232-7

Panzeri, S., Treves, A., 1996. Analytical estimates of limited sampling biases in different information measures. Network: Computation in Neural Systems 7, 87–107. https://doi.org/10.1080/0954898x.1996.11978656

Quian Quiroga, R., Nadasdy, Z., Ben-Shaul, Y., 2009. Unsupervised spike detection and sorting with wavelets and superparamagnetic clustering. Neural Comput 16, 1661–1687. https://doi.org/10.1162/089976604774201631

Reyes-Puerta, V., Sun, J.-J., Kim, S., Kilb, W., Luhmann, H.J., 2015. Laminar and columnar structure of sensory-evoked multineuronal spike sequences in adult rat barrel cortex in vivo. Cerebral Cortex 25, 2001–21. https://doi.org/10.1093/cercor/bhu007

Romo, R., Hernández, A., Zainos, A., Lemus, L., Brody, C.D., 2002. Neuronal correlates of decision-making in secondary somatosensory cortex. Nat Neurosci 5, 1217–25.

Rossant, C., Kadir, S.N., Goodman, D.F.M., Schulman, J., Hunter, M.L.D., Saleem, A.B., Grosmark, A., Belluscio, M., Denfield, G.H., Ecker, A.S., Tolias, A.S., Solomon, S., Buzski, G., Carandini, M., Harris, K.D., 2016. Spike sorting for large, dense electrode arrays. Nat Neurosci 19, 634–641. https://doi.org/10.1038/nn.4268

Salinas, E., Thier, P., 2000. Gain modulation: a major computational principle of the central nervous system. Neuron 27, 15–21.

Saxena, S., Cunningham, J.P., 2019. Towards the neural population doctrine. Curr Opin Neurobiol 55, 103–111.

Schmitzer-Torbert, N., Jackson, J., Henze, D., Harris, K., Redish, A.D., 2005. Quantitative measures of cluster quality for use in extracellular recordings. Neuroscience 131, 1–11. https://doi.org/10.1016/j.neuroscience.2004.09.066

Starosta, S., Güntürkün, O., Stüttgen, M.C., 2013. Stimulus-response-outcome coding in the pigeon nidopallium caudolaterale. PLoS One 8, e57407.

Starosta, S., Stüttgen, M.C., Güntürkün, O., 2014. Recording single neurons' action potentials in freely moving pigeons across three stages of learning. Journal of Visualized Experiments 88, e51283.

Steinmetz, N.A., Aydin, C., Lebedeva, A., Okun, M., Pachitariu, M., Bauza, M., Beau, M., Bhagat, J., Böhm, C., Broux, M., Chen, S., Colonell, J., Gardner, R.J., Karsh, B., Kostadinov, D., Mora-Lopez, C., Park, J., Putzeys, J., Sauerbrei, B., van Daal, R.J.J., Vollan, A.Z., Welkenhuysen, M., Ye, Z., Dudman, J., Dutta, B., Hantman, A.W., Harris, K.D., Lee, A.K., Moser, E.I., O'Keefe, J., Renart, A., Svoboda, K., Häusser, M., Haesler, S., Carandini, M., Harris, T.D., 2021. Neuropixels 2.0: A miniaturized high-density probe for stable, long-term brain recordings. Science (1979) 372. https://doi.org/10.1101/2020.10.27.358291

Stoilova, V. V, Knauer, B., Berg, S., Rieber, E., Jäkel, F., Stüttgen, M.C., 2020. Auditory cortex reflects goal-directed movement but is not necessary for behavioral adaptation in sound-cued reward tracking. J Neurophysiol 124, 1056–1071. https://doi.org/10.1152/jn.00736.2019

Stringer, C., Pachitariu, M., 2024. Analysis methods for large-scale neuronal recordings. Science (1979) 386. https://doi.org/10.1126/science.adp7429

Stringer, C., Zhong, L., Syeda, A., Du, F., Kesa, M., Pachitariu, M., 2025. Rastermap: a discovery method for neural population recordings. Nat Neurosci 28, 201–212. https://doi.org/10.1038/s41593-024-01783-4

Stüttgen, M.C., Schwarz, C., 2010. Integration of vibrotactile signals for whisker-related perception in rats is governed by short time constants: comparison of neurometric and psychometric detection performance. Journal of Neuroscience 30, 2060–9.

Stüttgen, M.C., Schwarz, C., 2008. Psychophysical and neurometric detection performance under stimulus uncertainty. Nat Neurosci 11, 1091–9.

Treves, A., Panzeri, S., 1995. The Upward Bias in Measures of Information Derived from Limited Data Samples. Neural Comput 7, 399–407. https://doi.org/10.1162/neco.1995.7.2.399

Unakafova, V.A., Gail, A., 2019. Comparing Open-Source Toolboxes for Processing and Analysis of Spike and Local Field Potentials Data. Front Neuroinform. https://doi.org/10.3389/fninf.2019.00057

van der Bourg, A., Yang, J.-W., Reyes-Puerta, V., Laurenczy, B., Wieckhorst, M., Stüttgen, M.C., Luhmann, H.J., Helmchen, F., 2017. Layer-Specific Refinement of Sensory Coding in Developing Mouse Barrel Cortex. Cerebral Cortex 27, 4835–50. https://doi.org/10.1093/cercor/bhw280

Vandevelde, J.R., Yang, J.-W., Albrecht, S., Lam, H., Kaufmann, P., Luhmann, H.J., Stüttgen, M.C., 2023. Layer- and cell-type-specific differences in neural activity in mouse barrel cortex during a whisker detection task. Cerebral Cortex 33, 1361–1382. https://doi.org/10.1093/cercor/bhac141

Yang, J.-W., Prouvot, P.-H., Stroh, A., Luhmann, H.J., 2017. Combining Optogenetics with MEA, Depth-Resolved LFPs and Assessing the Scope of Optogenetic Network Modulation, in: Optogenetics: A Roadmap. Springer Science & Business Media. https://doi.org/10.1007/978-1-4939-7417-7

Yeganeh, F., Knauer, B., Backhaus, R.G., Yang, J.W., Stroh, A., Luhmann, H.J., Stüttgen, M.C., 2022. Effects of optogenetic inhibition of a small fraction of parvalbumin - positive interneurons on the representation of sensory stimuli in mouse barrel cortex. Sci Rep 12, 19419. https://doi.org/10.1038/s41598-022-24156-y

Acknowledgments

Preparation of the toolbox and the manuscript were supported by several grants from the Deutsche Forschungsgemeinschaft to MCS (project IDs 179167628, 197059818, 223368015, 280347763, 424828846, and 543128862). The author is grateful for the feedback and support of present and former lab members. The LFP data were provided by Dr Jenq-Wei Yang and collected in the lab of Prof Heiko Luhmann, Institute of Physiology, University Medical Center Mainz, and are used with the authors' permission.

Figure legends

Figure 1. Flow chart for single-unit analysis and which MLIB functions to use at what stage of analysis.

Figure 2. Illustration of some MLIB functions to examine spike sorting quality (functions mcc, mcheck, mwave). A) All 853 waveforms from a sparsely firing single unit recorded in the pigeon nidopallium caudolaterale (gray), mean waveform (thick black line) and ±2 standard deviations (thin black lines). ADC, analog-to-digital conversion (depends on the units of voltage supplied by the user. B) Time-voltage heat map of the waveforms in A. C) Distributions of baseline (blue) and peak voltages (green: minima, red: maxima). The black normal curve was fitted to the green distribution and is used to estimate false negatives. Due to a conservative detection threshold (dotted line), the green distribution appears truncated (arrow), leading to missed spikes (estimate false-negative rate: 2%). D) Inter-spike interval histogram. Gray shaded area highlights period of 4 ms in which no spikes are expected. The fraction of spikes occurring in this interval should be near zero for clean single units. E) Stability of firing can be assessed by plotting the cumulative spike count over session time. Diagonal black dotted line for comparison to expected steady firing rate. F) Stability of the unit can further be assessed by plotting the spike waveform amplitude averaged over 1-minute bins as a function of time (thick red line). Thin red lines represent ±1 standard deviation. G) Similar to E and F, but plotting binned spike counts (bin size 1 minute) and all spike amplitudes (red dots) as a function of session time. The regression line suggests an average increase of spike amplitude (which however amounts to only 0.8 ADC units per minute). H) Some quality indices returned by mcheck. SNR(d), signal-to-noise-ratio, measured as the distance between the maximum and the minimum of the average waveform, divided by the pooled 99%-Winsorized standard deviation. CV(FR) and CV(amps) represent the coefficient of variation of the firing rate and the amplitudes and serve as stability indicators (see documentation for details). I) Waveform features extracted with mwave. FWHMax and FWHMin, full width at half maximum and minimum, respectively. P2TDur, P2TRat, P2TAmp,

peak-to-trough duration, ratio, and amplitude, respectively. J) Waveforms from two clusters of putative single units obtained from spike sorting. K) Waveforms plotted in principal component (PC) space. The first three PCs explain 44.8% of the total variance. Each dot represents a waveform. Bold points represent cluster means, ellipses represent the estimated covariance matrix (i.e., one standard deviation of a 2D Gaussian curve expressed as Mahalanobis distance in 2D space). L) Histogram of differences between the distance to the two cluster means for each waveform, plotted separately for the two clusters. Perfect cluster separation is achieved if the two distributions show zero overlap (i.e., no positive values of cluster 1 and no negative values of cluster 2). Class 1 and class 2 hit rates are proportions of correctly classified spikes for all possible values of D_1–D_2. Values of D can be understood as standard deviations in PC space, expressed as Mahalanobis distances. A' represents the area under the ROC curve which can be maximally 1; excellent cluster separability is achieved at values of A'>0.98, while values <0.8 indicate very poor cluster separability. M) mcc returns several standard unit isolation quality measures. Panels A through I are modified from mcheck output, panels J through M from mcc output.

Figure 3. Illustration of some MLIB functions pertaining to single-neuron spike train analysis (functions mpsth, msdf, mlat, mwa, mmultregress). A) Peri-stimulus time histogram and raster plot of a single neuron from rat auditory cortex (mpsth). The yellow line represents a spike density function generated by msdf, using an exponentially modified Gaussian kernel with SD = 1 ms and tau = 5 ms. The three colored points between the two subpanels mark different estimates of response latency returned by mlat. B) Sliding window analysis results (mwa). C) Multiple regression analysis of spike counts on three different predictors (mmultregress). Spike counts of a rat medial frontal cortex neuron recorded during execution of a single-interval forced choice auditory discrimination task were subjected to regression analysis with the binary predictors stimulus, response, and reward, computed in successive windows shifted by 25 ms, with three different analysis window durations (25 ms, 100 ms, 250 ms). Spike counts were normalized before regression was performed. Top row

shows the regression coefficients (intercept omitted), bottom row shows the squared semipartial correlation coefficient between each predictor and spike count, for each analysis window.

Figure 4. Illustration of dimensionality reduction for multi-neuron recordings (function mdimreduct). A) Average neuronal activity (z-scored and color-coded) for 300 neurons from medial frontal cortex around onset of an auditory stimulus (one of two), sorted by peak latency. B) The first 16 principal components (PCs) computed from the data in panel A. C) Percentage explained variance by the first 16 principal components (bars). Red line shows cumulated percentage. The first five PCs together explain roughly 78% of the variance. C) Population trajectory for the first three PCs. Time is color-coded from black (-400 ms relative to stimulus onset) to white (+400 ms). E) Same as panel D, but after dimensionality reduction for both stimuli together. The trajectories for the two types of trials begin to diverge shortly after stimulus onset (time point 0 marked by arrow).

Figure 5. Illustration of MLIB function mcsd for LFP data. A) Laminar LFP recordings in mouse barrel cortex after deflection of the principal whisker. Each line represents the average over 10 stimulus repetitions for one of 20 electrodes from a linear array (electrode spacing 50 µm). B) Same data as in panel A, but plotting distance of the electrodes from the pial surface on the ordinate. Average LFP responses are shown both as lines and pseudocolored (in mV). C) Current source density (CSD) plots for the data in panels A and B. Left: raw CSD, right: CSD after 10-fold spatial interpolation. Pseudocolor scale units are mV/mm^2. This data was collected by Dr Jenq-Wei Yang in the lab of Prof. Heiko Luhmann, University Medical Center Mainz, and is part of a larger data set published in (van der Bourg et al., 2017). The authors kindly granted permission to use this data in the present publication.

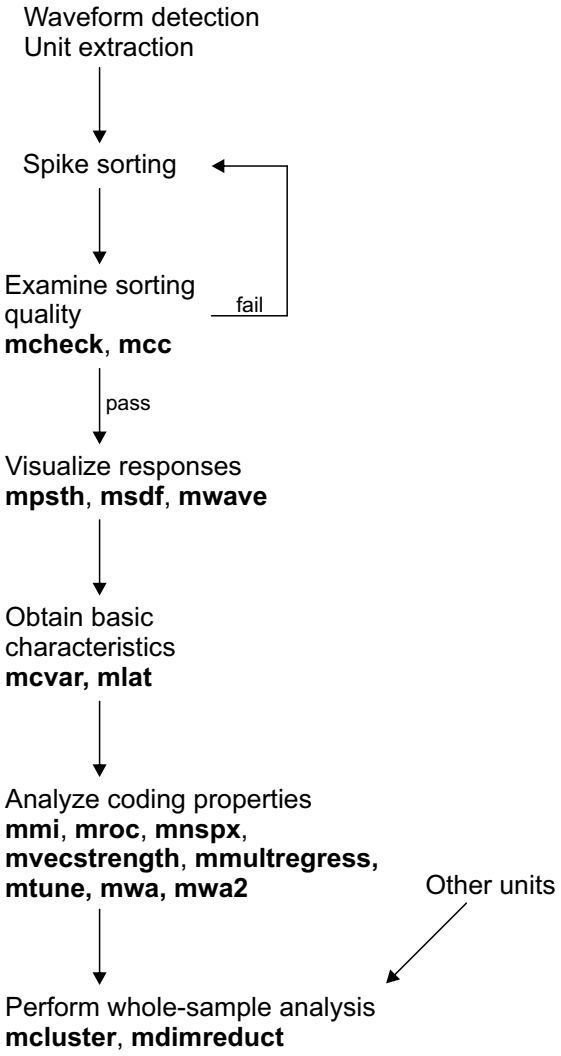
Waveform detection
Unit extraction
Spike sorting
Examine sorting quality
mcheck, **mcc**
fail
pass
Visualize responses
mpsth, **msdf**, **mwave**
Obtain basic characteristics
mcvar, mlat
Analyze coding properties
mmi, **mroc**, **mnspx**, **mvecstrength**, **mmultregress, mtune, mwa, mwa2**
Other units
Perform whole-sample analysis
mcluster, **mdimreduct**

Figure 1

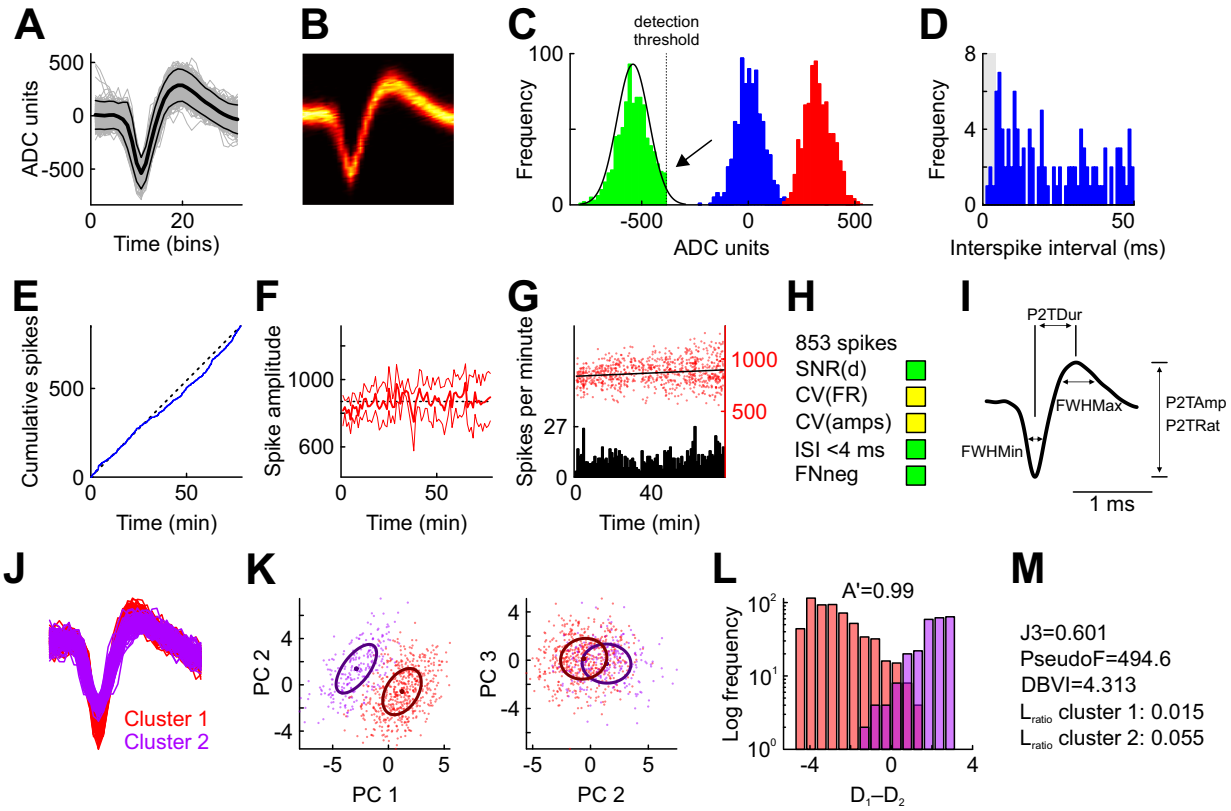
A
ADC units
500
0
-500
0
20
Time (bins)
B
C
detection threshold
Frequency
100
0
-500
0
500
ADC units
D
Frequency
8
4
0
0
50
Interspike interval (ms)
E
Cumulative spikes
500
0
0
50
Time (min)
F
Spike amplitude
1000
600
0
50
Time (min)
G
Spikes per minute
1000
500
27
0
0
40
Time (min)
H
853 spikes
SNR(d)
CV(FR)
CV(amps)
ISI <4 ms
FNneg
I
P2TDur
FWHMax
FWHMin
P2TAmp
P2TRat
1 ms
J
Cluster 1
Cluster 2
K
PC 2
4
0
-4
-5
0
5
PC 1
PC 3
4
0
-4
-5
0
5
PC 2
L
A'=0.99
Log frequency
10^2
10^1
10^0
-4
0
4
D_1–D_2
M
J3=0.601
PseudoF=494.6
DBVI=4.313
L_{ratio} cluster 1: 0.015
L_{ratio} cluster 2: 0.055

Figure 2

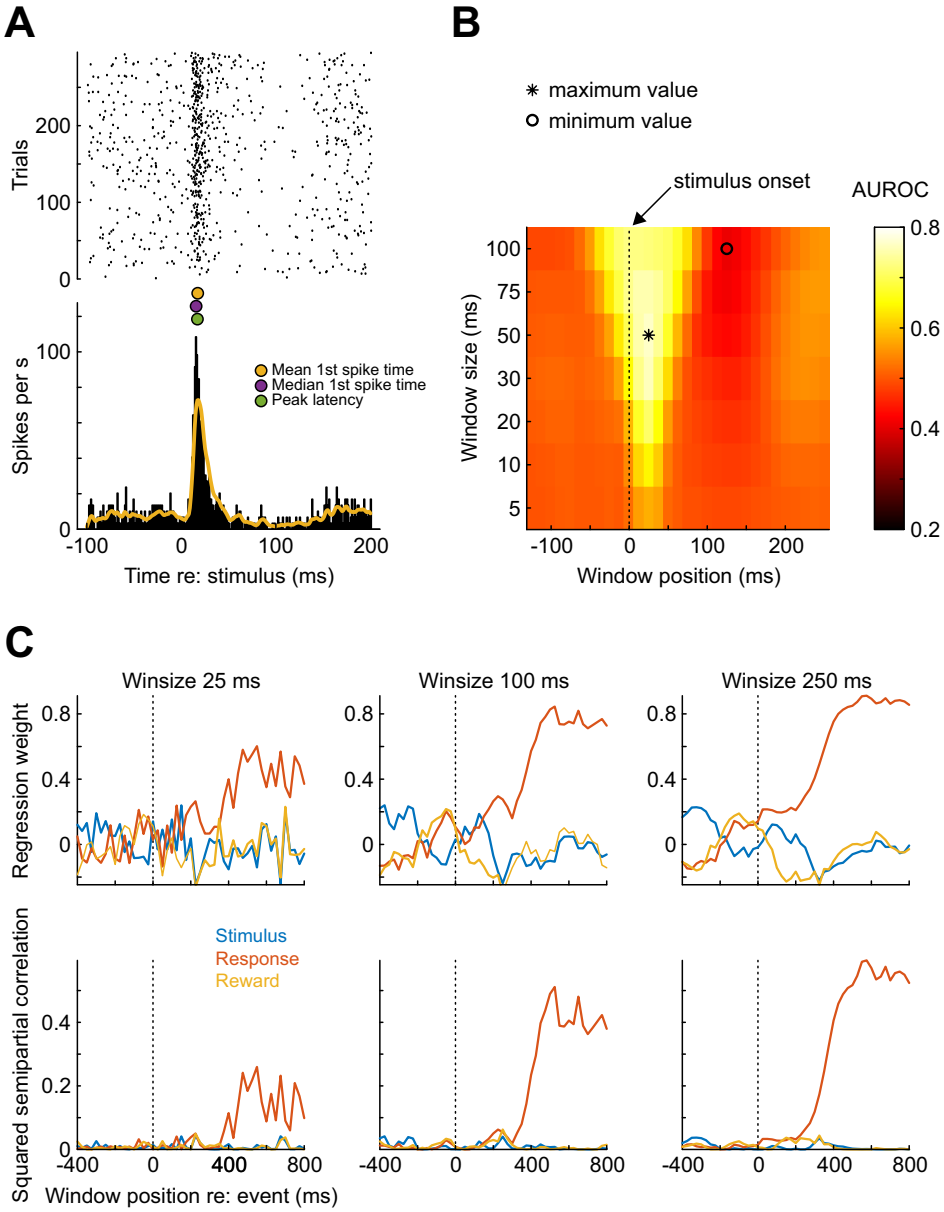
A
Trials
200
100
0
Spikes per s
100
0
Mean 1st spike time
Median 1st spike time
Peak latency
-100
0
100
200
Time re: stimulus (ms)
B
maximum value
minimum value
stimulus onset
AUROC
0.8
0.6
0.4
0.2
Window size (ms)
100
75
50
30
20
10
5
-100
0
100
200
Window position (ms)
C
Winsize 25 ms
Winsize 100 ms
Winsize 250 ms
Regression weight
0.8
0.4
0
Stimulus
Response
Reward
Squared semipartial correlation
0.4
0.2
0
-400
0
400
800
Window position re: event (ms)

Figure 3

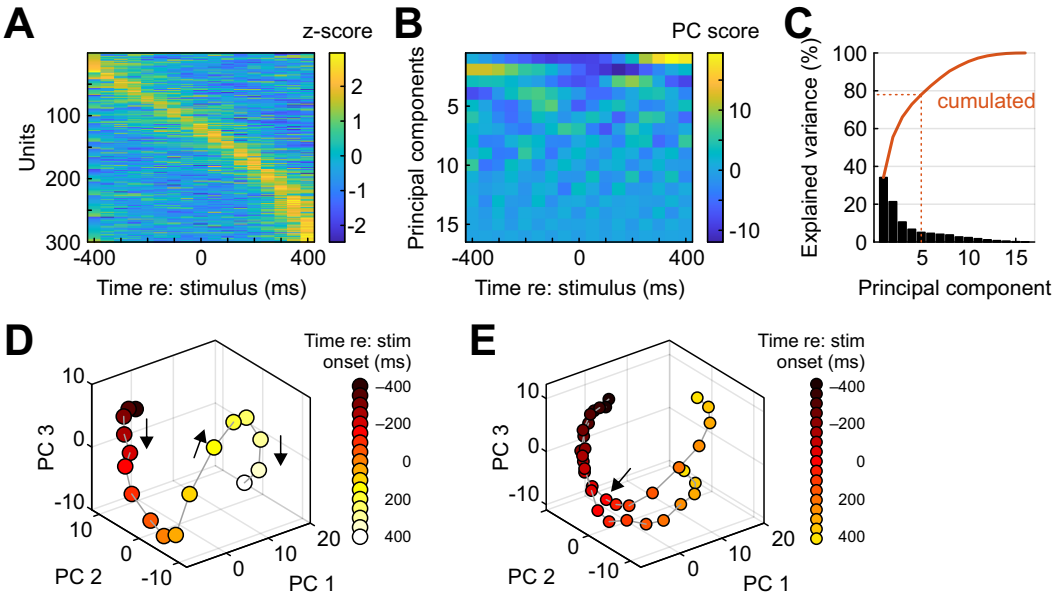
A
z-score
Units
100
200
300
-400
0
400
Time re: stimulus (ms)
2
1
0
-1
-2
B
PC score
Principal components
5
10
15
-400
0
400
Time re: stimulus (ms)
10
0
-10
C
Explained variance (%)
100
80
60
40
20
0
cumulated
5
10
15
Principal component
D
Time re: stim onset (ms)
PC 3
PC 2
PC 1
10
0
-10
20
-400
-200
0
200
400
E
Time re: stim onset (ms)
PC 3
PC 2
PC 1
10
0
-10
20
-400
-200
0
200
400

Figure 4

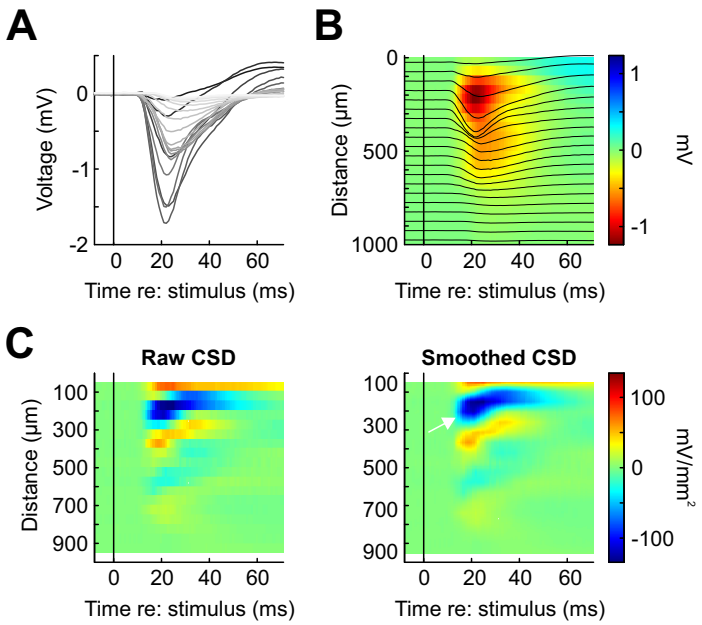
A
Voltage (mV)
0
-1
-2
0 20 40 60
Time re: stimulus (ms)
B
Distance (µm)
0
500
1000
0 20 40 60
Time re: stimulus (ms)
1
0
-1
mV
C
Raw CSD
Smoothed CSD
Distance (µm)
100
300
500
700
900
0 20 40 60
Time re: stimulus (ms)
100
0
-100
mV/mm²

Figure 5